Two Dimensional Model of an Electro-Thermal Ice Protection System

L. Bennani*
Airbus Operations SAS, Toulouse, 31000, France

P. Villedieu†
ONERA, Toulouse, 31000, France

M. Salaun‡
ISAE, Toulouse, 31000, France

In this communication we shall focus on the main governing equations and building blocks of the M.A.D (Anti-icing Deicing Modelling) numerical tool, which is now renamed as INUIT (Integrated NUmerical model of Ice protection sysTems) and part of the new generation of ONERA icing codes. The code simulates the functioning of an electro-thermal de-icing system. We shall also discuss the various improvements and new features we have added, especially a mechanical model of the ice block in order to improve the ice-shedding criterion.

I. Introduction

In the aeronautical world, icing is one of the most serious hazards that can be encountered. Icing is caused by freezing upon impact of supercooled water droplets. Not only does it increase mass but it may also lead to a degradation of aerodynamic performances, blocked air intakes and in the worst case, loss of control of the aircraft. Aircraft manufacturers must therefore comply with certifications and regulations regarding flight safety in icing conditions. In order to achieve that goal several ice protection technologies may be adopted. A popular system is the bleed air anti-icing system, where hot air is taken from the engine to heat the desired protected surfaces so as to prevent the formation of ice. However nowadays aircraft manufacturers are moving towards more economic, green and electrical aircraft. In this context a possible candidate is the electro-thermal ice protection system, which relies on cyclic heater mat activation to detach the ice.

This calls for numerical tools in order to assist the manufacturer during the design phase of these ice protection systems so as to assess their performances and suitability. Moreover it is most important to be able to predict the ice shape and the performance degradation it causes. In this context, a new generation of icing codes are being developed at ONERA. The ONERA 2D icing codes are currently being updated to more modern numerical methods and programming architectures. The work presented here concerns the updating and development of new models in the electro-thermal ice protection system simulation module. Figure 1 gives a schematic view of the new code's intended architecture:

*Phd Student, EGAMT
†Senior scientist, DMAE-MH, AIAA Member
‡Professor, DMSM

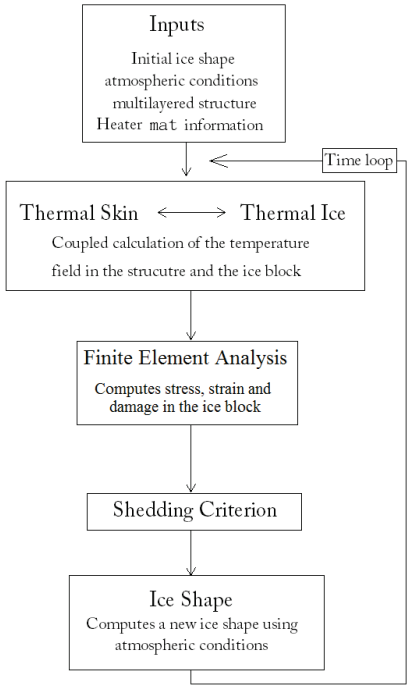

Figure 1. The code's architecture

In the following sections, we will first describe the way of approaching the different heat transfer problems. Then we will describe how we intend to tackle the ice shedding problem.

II. The electro-thermal system

The system we are trying to model is composed of heater mats installed within a multi-layered material and can be used in anti-icing or deicing configurations.[9,23] These mats are activated according to a predefined time dependent cycle in order to melt some regions of the ice at the ice/structure interface. This will reduce the ability of the ice to adhere to the surface and will lead to shedding. At the time being the system is modeled in two dimensions. Figure 2 gives an illustration of the system.

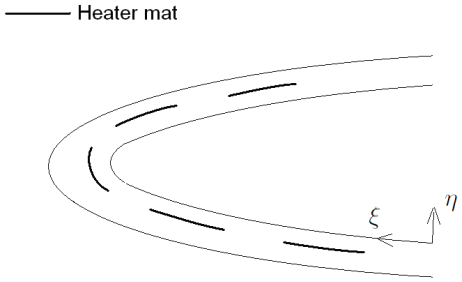

Figure 2. Illustration of a leading edge electro-thermal ice protection system

As the structure containing the system remains fixed, only the ice block's frontier will be subject to change in time. Thus considering each domain has its own geometrical behaviour in time, it seems reasonable to treat them separately. What we mean by "separately" is that the meshes will be generated differently and separate modular blocks will be assigned in the code to treat each domain. However the physics will be

treated simultaneously by a coupling procedure at the ice/structure interface.

III. Heat transfer in the (multi-layered) structure

III.A. Physical process and modelling

Here we must solve the problem of heat conduction, governed by the heat equation (eq 1), in a structure composed of different materials and with localized heat sources provided by the heating mats.

$$\rho c_p \frac{\partial T}{\partial t} + \nabla . \left(-\Lambda \overrightarrow{\nabla T} \right) = S \tag{1}$$

Thus on the one hand changes in material characteristic constants such as density and specific heat must be handled. On the other hand the heating mats are not explicitly represented as a part of the calculation domain and their presence must be modelled. Thermal conductivity is allowed to be anisotropic, having different conductivities along ξ and η (where (ξ,η) is a curvilinear coordinate system as illustrated figure 2). Therefore the thermal conductivity matrix Λ has the form:

$$\begin{pmatrix} \lambda_\xi & 0 \\ 0 & \lambda_\eta \end{pmatrix}$$

We then proceed to a discretization of equation 1 that we solve with a finite volume method. We choose an implicit time marching algorithm due to the fact that some materials in the structure may be very good conductors. Indeed, this would put a harsh limit to the authorised value of the time step had we chosen an explicit formulation. The heating mats are considered to be located at the interface between two layers and are not explicitly meshed. In order to take into account their presence the product ρc_p of each adjacent cell is modified according to the following formula, defining an equivalent ρc_p:[9]

$$(\rho c_p)_{eq} = \frac{(\rho c_p)_j \, e_j + (\rho c_p)_r \, e_r/2}{e_j + e_r/2} \tag{2}$$

Where e_j and e_r are the thickness of the adjacent cell and the heating element respectively. If P is the power of the heating element, the heat provided is represented as a heat source $S_j = \frac{P}{2}$ in each adjacent cell. We assume perfect thermal contact between layers, but this assumption could easily be extended to non perfect contact in a future version of the code. Figure 3 shows an instantaneous shot of the temperature field in the structure taken during a de-icing cycle. We can clearly see the zones where the heater pads are active at that instant.

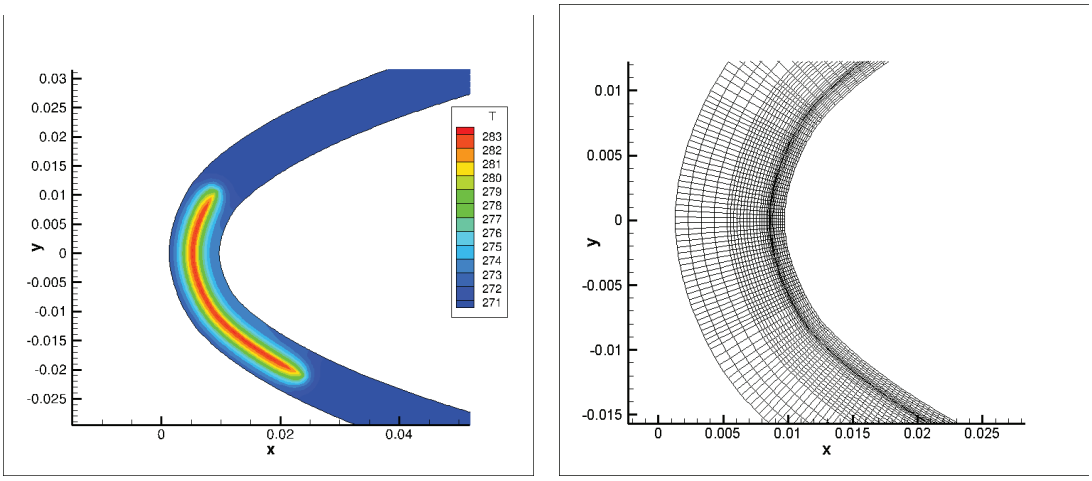

(a) Temperaure field in K (b) Mesh

Figure 3. Example of temperature field and mesh in the structure

III.B. Academic validation case

As a first step of validation we consider a simple geometry, a hollow cylinder, made of a single material, which has a fixed uniformly distributed temperature T_o on its inner and outer surfaces and a uniform initial temperature field T_i (see figure 4).

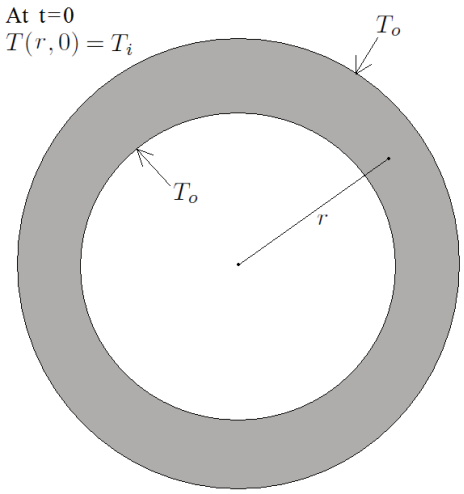

Figure 4. Illustration of the hollow cylinder academic case

The analytic solution, given in,[22] is a temperature field that depends only on the radial coordinate r and time.

$$\frac{T - T_o}{T_i - T_o} = \pi \sum_{n=1}^{+\infty} f(R, \lambda_n) e^{-\lambda_n \frac{\alpha t}{r_o}} \tag{3a}$$

$$f(R, \lambda_n) = \frac{J_0(\lambda_n R_i)\left[J_0(\lambda_n R) Y_0(\lambda_n) - J_0(\lambda_n) Y_0(\lambda_n R)\right]}{J_0(\lambda_n R) + J_0(\lambda_n)} \tag{3b}$$

$$J_0(\lambda_n R_i) Y_0(\lambda_n) - J_0(\lambda_n) Y_0(\lambda_n R_i) = 0 \tag{3c}$$

$$R = \frac{r}{r_o} \tag{3d}$$

We compare this solution to the solution obtained by the heat transfer module at different times. As shown on figure 5 we have a very good match between the analytic and computed profiles.

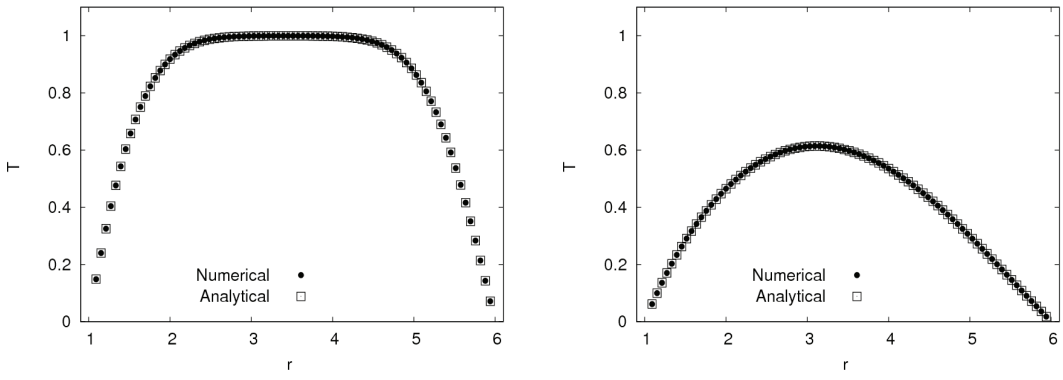

(a) At $t = 0.2s$ (b) At $t = 2.0s$

Figure 5. Comparison of non-dimensional analytic and computed temperature profiles

IV. Heat transfer in the ice block

IV.A. Physical process and modelling

In the ice block the material remains the same over the whole domain, that is to say, water. The specific physical process that arises when dealing with this domain is phase change. This mechanism involves a discontinuous enthalpy-temperature relation. In order to capture this discontinuity many methods exist (eg : level set, phase field). In our case the so called enthalpy method is chosen. This method enables an efficient capturing of the melting front.[1] The main idea is to return to the general energy conservation equation :

$$\int_t^{t+\Delta t} \frac{\partial}{\partial t}\left[\int_V \rho h dV\right] dt = \int_t^{t+\Delta t} \int_{\partial V} -\overrightarrow{q}\cdot\overrightarrow{n}\, dS dt \tag{4}$$

The heat flux $\overrightarrow{q}$ is computed using the temperature field. Knowing the flux then enables us to update the value of the enthalpy. The following relationship (5) then gives us the new values of temperature :

$$T = \begin{cases} T_m + \frac{h}{c_s} & h \leq 0 \\ T_m & 0 \leq h \leq L \\ T_m + \frac{h-L}{c_l} & h \geq L \end{cases} \tag{5}$$

and we can update the liquid fraction, which is a crucial element for computing the heat fluxes :

$$\phi_L = \begin{cases} 0 & h \leq 0 \\ \frac{h}{L} & 0 \leq h \leq L \\ 1 & h \geq L \end{cases} \tag{6}$$

Here the following convention has been chosen for h :

$$h = \begin{cases} c_s\,(T - T_m) & T < T_m \text{ solid} \\ \phi_L L & T = T_m \text{ mixed state} \\ c_l\,(T - T_m) + L & T < T_m \text{ liquid} \end{cases} \tag{7}$$

In this approach the density ρ is assumed constant (and the same for water in both solid and liquid states). The equations are solved using an explicit time stepping finite volume method. In this case the explicit formulation is justified by the fact that ice and water are not very good heat conductors. Therefore the time step is not too limited by the stability condition. The open source meshing software Triangle is used to generate the unstructured mesh.[21] Figure 6 shows preliminary results of this module. An instantaneous shot of a phase indicator (liquid fraction) field is represented. We clearly see the formation of a liquid water film at the heated surface.

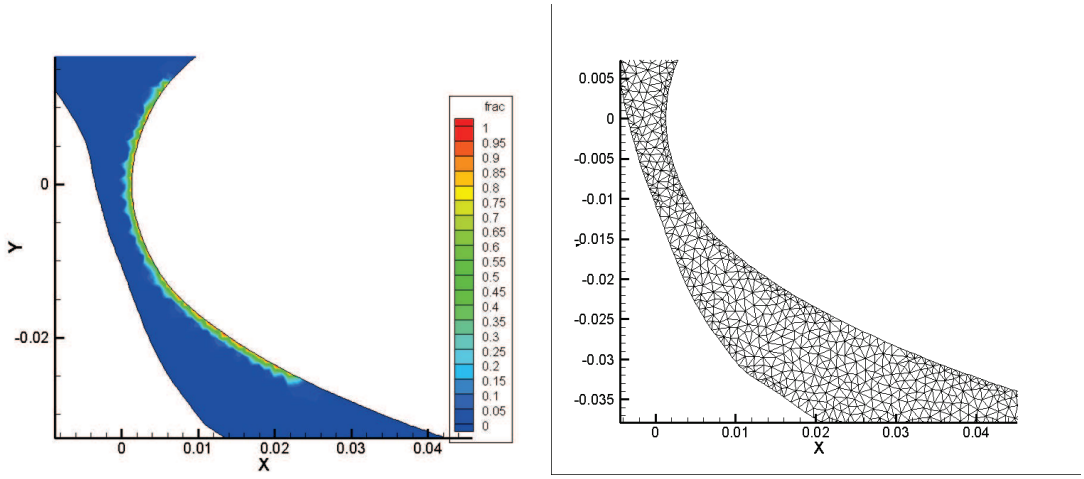

(a) Phase indicator (b) Mesh

Figure 6. Phase indicator and mesh of the ice block

IV.B. Academic validation case

As in the case of the heat transfer in the structure (section III.B) we would first like to know if our numerical procedure correctly solves the mathematical equations used to model our problem. In this case we are going to consider the case of a rectangular slab of ice uniformly heated at one of its surfaces. The other boundaries are assumed adiabatic. The case is illustrated fig 7.

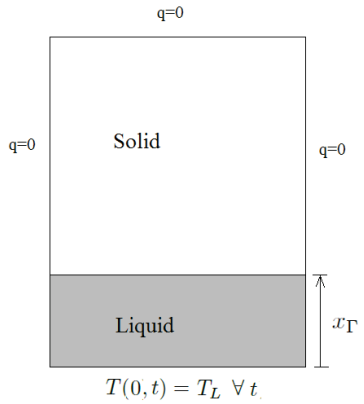

Figure 7. Phase change academic case

The problem reduces itself to a one dimensional one, for which analytic solutions are available.[1] In this case the position of the melting front is given by:

$$x_\Gamma(t) = 2\chi\sqrt{\alpha_l t} \tag{8}$$

Where χ is the solution of the transcendental equation :

$$\frac{St_l}{e^{\chi^2} erf(\chi)} - \frac{St_s}{\nu e^{\nu^2\chi^2} erfc(\nu\chi)} = \chi\sqrt{\pi} \tag{9}$$

With

$$St_l = \frac{c_l(T_L - T_m)}{L} \qquad St_s = \frac{c_s(T_m - T(x,0))}{L} \qquad \nu = \sqrt{\frac{\alpha_l}{\alpha_s}} \tag{10}$$

In order to compare the analytic and numerical results we perform an integration of the numerical liquid fraction over the whole domain. The result is then divided by the thickness of the slab. This gives us the position x_Γ of the melting front. The time dependent positions of these fronts are shown figure 8. We observe a good match between analytic and numerical results, although the two curves tend to very slightly drift apart with time.

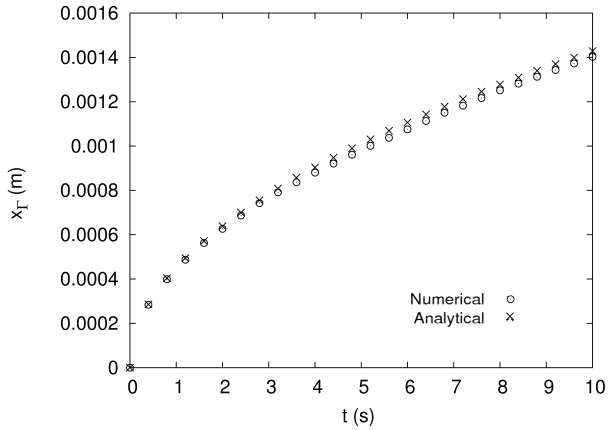

Figure 8. Comparison of melting front positions

V. Mechanical models and ice shedding

Once we have determined the regions of the ice block which have melted and the global temperature field, we must predict if ice shedding occurs or not. To do so an empirical model was originally used in the code, as we will see in section V.A. Nevertheless such a criterion is unsatisfactory since it does not take into account aerodynamic and inertial forces (ex: for rotating blades).

Modelling techniques based on continuum mechanics have already been applied to ice. Scavuzzo *et al.* performed a finite element analysis of the stress distribution due to aerodynamic forces in an accreted ice block.[18] More recently Zhang *et al.* have used a crack propagation and re-meshing technique to study ice break up.[19]

As for adhesion, in a general way, there are several identified mechanisms (mechanical interlocking, electrostatic attraction, chemical, adhesion by diffusion[20]). The problem is then to identify by which of these mechanisms ice adheres to a surface. Some theoretical models have been proposed to explain and predict ice adhesion. One assumes the existence of a liquid like layer on ice.[13,14] Another is a model based on the electrostatic adhesion mechanism.[10] In addition, Fortin and Perron have recently developed an ice adhesion model based on electrostatic and mechanical interlocking mechanisms.[8]

Although the adhesion models cited previously are based on more fundamental physical considerations, in our work we adopt a more global approach based on continuum damage mechanics.

One of the main problems that arises now is to determine what mechanical properties we are going to use in order to characterise atmospheric ice, for unfortunately very few studies on the subject exist. Most studies are interested in the tensile or compressive strength but do not provide many information on mechanical characteristics.[2,11,15] Moreover these experiments are very difficult to conduct due to the vast number of parameters on which those properties depend. Eskandarian[7] reports experimental measurements of Young's modulus and Poisson's ratio for porous ice. These results could be used for rime ice, in which small air bubbles are trapped, but this would require us to know the actual value of the porosity. Thus we see that it is very complicated to correctly describe the mechanical properties of atmospheric ice.

Therefore as a first approach we will use the values given by experiments for natural ice, which are more precise, and more widely studied. According to Schulson and Duval[6] the most precise results were obtained by Gammon *et al.*[17] In the case of a homogeneous polycrystalline ice aggregate, it may be assumed that the grains (crystallites) are oriented randomly making it elastically isotropic. The parameters characterising homogeneous isotropic elastic behaviour of polycrystalline ice Ih are shown in the following table (1)[6]:[17]

Property	Units	Value
Young's modulus, E	$N.m^{-2}$	$9.33\,10^9$
Poisson's ratio, ν	$\varnothing$	0.325

Table 1. Elastic constants of interest for isotropic polycrystalline Ice Ih at $T = -16°C$

The temperature dependence of these constants is obtained using the formulas given in,[6] however in this first approach we will neglect the effects of temperature on mechanical properties.

As for the fracture toughness, according to the data presented in,[6] we choose a value of $100kPa/m^{-1/2}$.

V.A. Empirical model

The ice adhesion model that was originally implemented in M.A.D is empirical. It states that if the ratio Lwf/Lt between water film length and total ice block length becomes greater than a certain user defined limit value (80% recommended) then the ice block detaches from the structure. A variant of this criterion based on the water film height is also implemented. These criteria illustrate the fact that ice adhesion is a very delicate mechanisms to model.

V.B. Linear elastic damage model

V.B.1. Presentation of the model

Brittle fracture is one of the most striking phenomena involved in ice shedding. Several approaches to fracture mechanics exist such as XFEM or remeshing. Here we chose to use a method that resembles those of continuum damage mechanics.

In the following paragraphs we are going to re-derive the equations obtained by Miehe *et al*[5] following an auxiliary (although closely related) method. The starting point is a principle of conservation of energy whose physical motivation is the following: when a solid is deformed by action of external forces it internally stores elastic deformation energy. If, locally, this energy exceeds a certain critical energy then it will go into creating an increase in crack surface. Therefore, if a crack nucleates and/or propagates, a possible mechanism (from a macroscopic point of view) could be a process of energy transfer from the applied forces to elastic deformation energy to crack surface energy.

The idea is to introduce a parameter d that characterises the local state of damage/fracture[12] in the ice block. Let's start by first stating the general equilibrium equations of continuum mechanics. Consider a domain Ω on which is applied a body force f_{vol} and a surface load f_{surf} on Γ_1. On Γ_2 the displacement field is imposed to u_d. Then we have :

$$\begin{aligned} -div(\sigma(u,d)) &= f_{vol} \quad && \text{in } \Omega \\ \sigma.n &= f_{surf} && \text{on } \Gamma_1 \\ u &= u_d && \text{on } \Gamma_2 \end{aligned} \tag{11}$$

Let $\psi(\epsilon, d)$ be the elastic deformation energy per unit volume, and $\phi(d, \nabla d)$ be the crack energy per unit volume. Therefore the total elastic energy will be $E_{el} = \int_\Omega \psi(\epsilon, d)dV$ and the total crack energy will be $E_{crack} = \int_\Omega \phi(d, \nabla d)dV$. In order to evaluate the energy dissipated by a crack Bourdin *et al*[3] have proposed a regularization of the crack surface density, given by the functional 12. According to Miehe *et al*[5] this is analogous to a phase-field model where d would be the order parameter.

$$\gamma(d, \nabla d) = \frac{1}{2l}d^2 + \frac{l}{2}\nabla d.\nabla d \tag{12}$$

The length scale l is a spreading parameter for the crack. The energy of fracture is obtained by multiplying this surface by g_c, the energy release rate, and is given by (13)

$$E_{crack} = \int_\Omega g_c[\frac{1}{2l}d^2 + \frac{l}{2}\nabla d.\nabla d]dV \tag{13}$$

When external forces are applied, the change in energy is equal to the work produced by those forces. Thus we have (14)

$$\delta E_{crack} + \delta E_{el} = \int_\Omega f_{vol}\delta u dV + \int_{\Gamma_1} f_{surf}\delta u d\Gamma \tag{14}$$

Using relation (13) and integrating by parts we find :

$$\delta E_{crack} = \int_\Omega \left[\frac{g_c}{l}d - g_c l\triangle d\right]\delta d dV + \int_{\partial\Omega} g_c l\nabla d.n\delta d d\Gamma \tag{15}$$

Using 15 and $\delta E_{el} = \int_\Omega \left[\frac{\partial\psi}{\partial\epsilon}\delta\epsilon + \frac{\partial\psi}{\partial d}\delta d\right]dV$ we find:

$$\int_\Omega \frac{\partial\psi}{\partial\epsilon}\delta\epsilon + \left[\frac{\partial\psi}{\partial d} + \frac{g_c}{l}d - g_c l\triangle d\right]\delta d dV + \int_{\partial\Omega} g_c l\nabla d.n\delta d d\Gamma = \int_\Omega f_{vol}\delta u dV + \int_{\Gamma_1} f_{surf}\delta u d\Gamma$$

Moreover, the mechanical boundary condition gives us :

$$\int_{\partial\Omega} f_{surf}\delta u d\Gamma = \int_{\partial\Omega} \sigma.n\delta u d\Gamma = \int_\Omega div(\sigma)\delta u dV + \int_\Omega \sigma : \nabla\delta u dV \tag{16}$$

As the Cauchy stress tensor is symmetric, we also have $\sigma : \nabla\delta u = \sigma : \delta\epsilon$. Therefore we get:

$$\int_\Omega f_{vol}\delta u dV + \int_{\partial\Omega} f_{surf}\delta u d\Gamma = \int_\Omega \left[div(\sigma) + f_{vol}\right]\delta u dV + \int_\Omega \sigma : \delta\epsilon dV$$

Given the mechanical equilibrium relation $div(\sigma) + f_{vol} = 0$, relation (14) reduces to :

$$\int_\Omega \left[\frac{\partial\psi}{\partial\epsilon} - \sigma\right]\delta\epsilon dV + \int_\Omega \left[\frac{\partial\psi}{\partial d} + \left[\frac{g_c}{l}d - g_c l\triangle d\right]\right]\delta d dV + \int_{\partial\Omega} g_c l\nabla d.n\delta d d\Gamma = 0$$

Thus we finally obtain (17) :

$$\begin{array}{ll} \sigma = \frac{\partial \psi}{\partial \epsilon} & \text{in } \Omega \\ -\frac{\partial \psi}{\partial d} = \frac{g_c}{l} d - g_c l \triangle d & \text{in } \Omega \\ \nabla d.n = 0 & \text{on } \partial\Omega \end{array} \tag{17}$$

We see that the stress tensor σ is deduced from the choice of ψ. In the case of linear isotropic homogeneous elasticity it is well established that ψ takes the form:

$$\psi(\epsilon) = \frac{\lambda}{2} tr(\epsilon)^2 + \mu tr(\epsilon^2) \tag{18}$$

However, considering $-\frac{\partial \psi}{\partial d}$ is the source term, the driving force of the fracture process, we must also chose ψ according to what part of the elastic deformation energy creates or propagates a crack. It is considered that a crack may nucleate or propagate only under local tension. Therefore ψ is decomposed into the sum of a tensile and a compressive part, which are defined by analogy with 18 and using the eigen values of ϵ as follows:

$$\psi_0^{+/-}(\epsilon) = \frac{\lambda}{2} < \epsilon_1 + \epsilon_2 >_{+/-}^2 + \mu(< \epsilon_1 >_{+/-}^2 + < \epsilon_2 >_{+/-}^2)$$

As fracture may only be influenced by the tensile energy, ψ is defined as:

$$\psi(\epsilon, d) = g(d)\psi_0^+(\epsilon) + \psi_0^-(\epsilon) \tag{19}$$

Where $g(d)$ represents the degradation of tensile energy due to crack formation. Therefore g is a non increasing function and we have $g(0) = 1$ and $g(1) = 0$. Moreover, when $d = 1$ it is asked that the driving force $-\frac{\partial \psi}{\partial d} = -g'(d)\psi_0^+(\epsilon)$ be equal to 0. To do so the additional condition $g'(1) = 0$ is imposed. Under these conditions Miehe *et al*[5] proposed the function $g(d) = (1-d)^2$. Using these new relations the complete set of equations becomes :

$$\begin{array}{ll} -div(\sigma(u,d)) = f_{vol} & \text{in } \Omega \\ \sigma.n = f_{surf} & \text{on } \Gamma_1 \\ u = u_d & \text{on } \Gamma_2 \\ \frac{g_c}{l} d - g_c l \triangle d = 2(1-d)\psi_0^+(\epsilon) & \text{in } \Omega \\ \nabla d.n = 0 & \text{on } \partial\Omega \end{array} \tag{20}$$

Equations 20 are nonlinear and describe a stationary damaged equilibrium state compatible with the external constraints. In order to solve these equations Miehe *et al*[5] have proposed an iterative procedure based on the introduction of a history function $\mathcal{H}$. $\psi_0^+(\epsilon)$ is then replaced by $\mathcal{H}$ in equation 20. The iterative process is solved by a finite element method[a] and defined by :

- Compute the history field:

$$\mathcal{H}^i = max(\mathcal{H}^{i-1}, \psi_0^+(\epsilon^{i-1})) \tag{21}$$

- Compute the damage field:

$$\begin{array}{ll} \frac{g_c}{l} d^i - g_c l \triangle d^i = 2(1-d^i)\mathcal{H}^i & \text{in } \Omega \\ \nabla d^i.n = 0 & \text{on } \partial\Omega \end{array} \tag{22}$$

- Compute the displacement field:

$$\begin{array}{ll} -div(\sigma^i(\epsilon^i, d^i) = f_{vol} & \text{in } \Omega \\ \sigma^i.n = f_{surf} & \text{on } \Gamma_1 \\ u^i = u_d & \text{on } \Gamma_2 \end{array} \tag{23}$$

[a] As a first approach we have simplified the constitutive law by considering that the damage coefficient affects both the tensile and compressive parts.

If we accept to consider the iterative process as pseudo-unsteady, it can be interpreted as follows: equations 20 only translate conservation of energy. At a given iteration i the tensile energy could locally be inferior to its value at iteration $i-1$. Thus if, at a given iteration, $d=1$, nothing is preventing it from decreasing at any following iteration. But clearly in our case, the problem of crack propagation is irreversible: d should not be allowed to decrease. Thus the history function $\mathcal{H}$ serves to take into account the irreversibility of the crack propagation process. It records, locally, the maximum of the tensile energy over all iterations. Intuitively, if at a given iteration there was enough tensile energy to increase the damage variable d, then this information will be contained in $\mathcal{H}$ for the following iteration. Nevertheless this is only true in a pseudo-iterative context, further investigation remains to be done in order to determine the exactitude of this interpretation.

V.B.2. Crack propagation test cases

In order to assess the quality of the results obtained via the model presented in section V.B, we performed test cases for which experimental results are available.[4,16]

First we consider a slab of brittle material, which has a vertical notch, on which we apply purely shear loads (mode II). This is one of the test cases presented by Miehe *et al.*[5] We also choose to use the same parameters for this test case. They are summarized in table 2. Figure 9(a) illustrates such a set up.

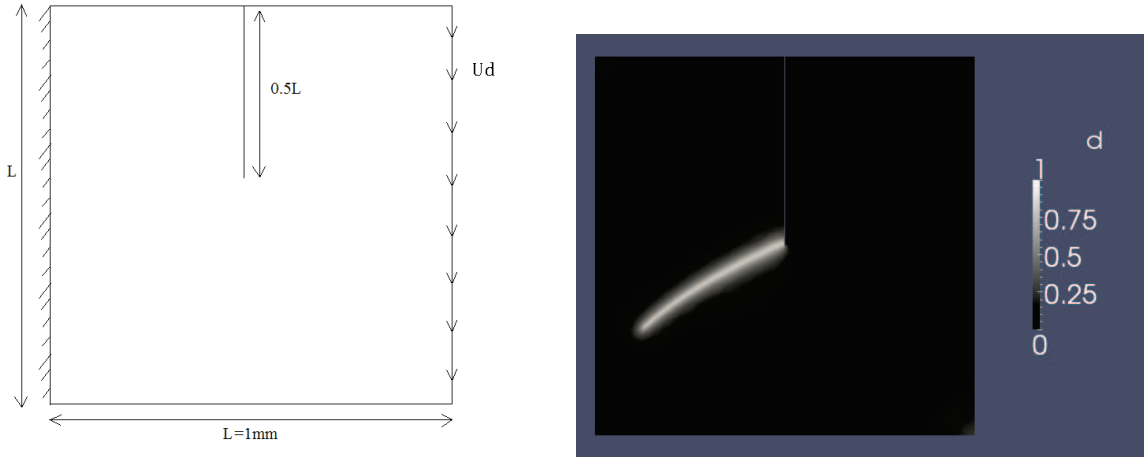

(a) Setup (b) Crack paths

Figure 9. Computational setup and results

Parameter	Unit	Value
u_d	m	13.410^{-6}
λ	GPa	$9.33\,10^{9}$
μ	GPa	121.15
g_c	$Pa.m^{-1/2}$	2700
l	m	$1.5\,10^{-5}$

Table 2. Computation parameters

On figure 9(b) we observe that the crack takes a curved path which is the awaited result. Indeed, this result is also observed experimentally.[16]

Next, let's consider a slab of brittle material, which has two horizontal notches, on which we apply loads both in tension and shear (mixed mode), as depicted figure 10(a). This time the mechanical properties are those of ice. The imposed displacement has value $u_d = 5.0\,10^{-6}m$ with $\theta = \pi/3$ and the length scale is set to $l = 7.5\,10^{-5}m$

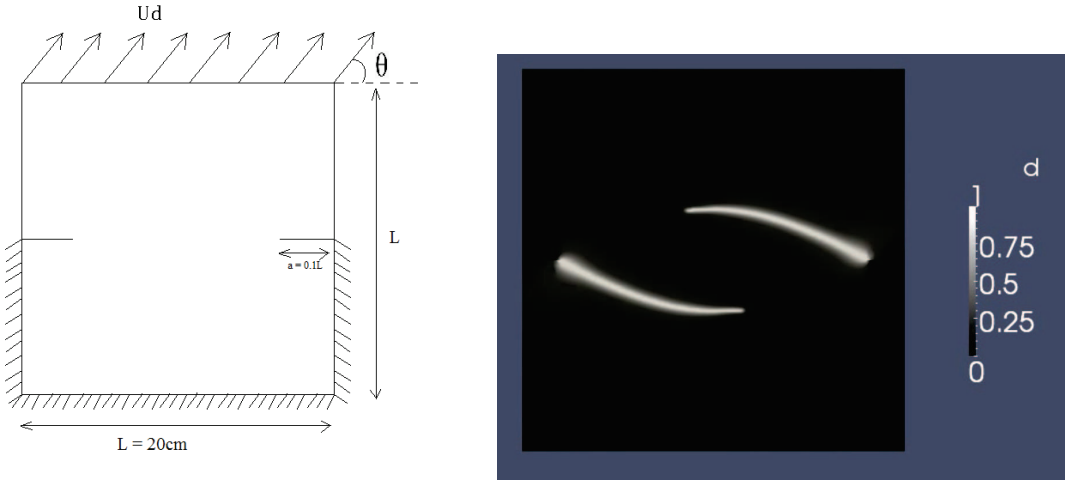

(a) Setup (b) Crack paths

Figure 10. Computational setup and results

The result of the computation is shown figure 10(b). The crack paths are once again those qualitatively observed in experiments using the same setup.[4]

VI. Simulation

VI.A. Thermal modules

The two thermal modules are explicitly coupled in order to compute the whole temperature field. On figure 11 we can clearly see the formation of the melted region (in white) corresponding to the activation of a heater mat. The snapshot is taken from a fictitious test case and serves only to prove feasibility.

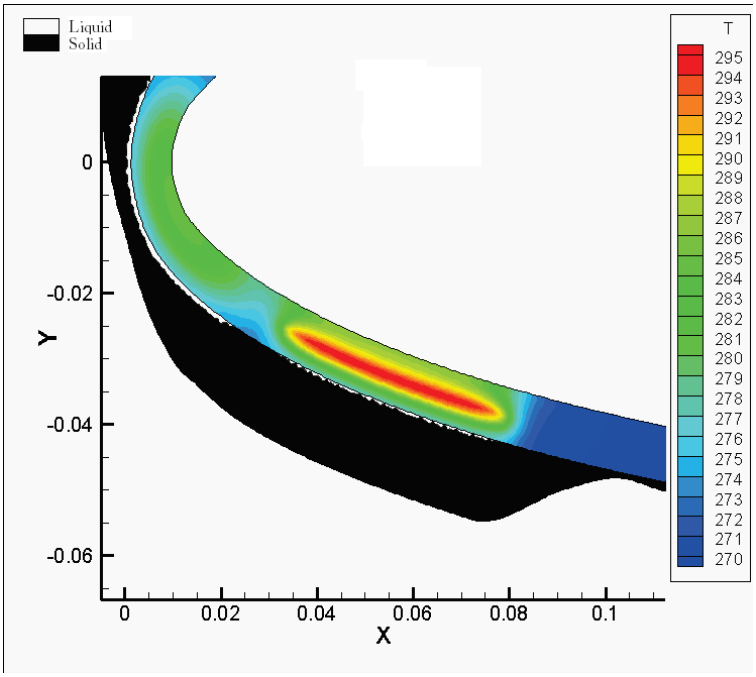

Figure 11. Thermal computation

However, although individual validation has been achieved on theoretical grounds for each module, the whole remains to be validated against experimental data.

VI.B. Ice shedding feasibility study

Here the goal is to study the feasibility of ice shedding prediction using the crack propagation model. To do so we consider a simplified situation. We obtain an ice shape and aerodynamic field with the accretion solver of the 2D suite. We then suppress a part of the ice at the leading edge so as to imitate a parting strip. Next we launch a thermal computation to predict the melted regions at the ice/surface interface. We then apply the aerodynamic loads and predict crack propagation. Figure 12 shows a crack that cuts through the ice shape, therefore demonstrating the feasibility of ice shedding prediction using this method.

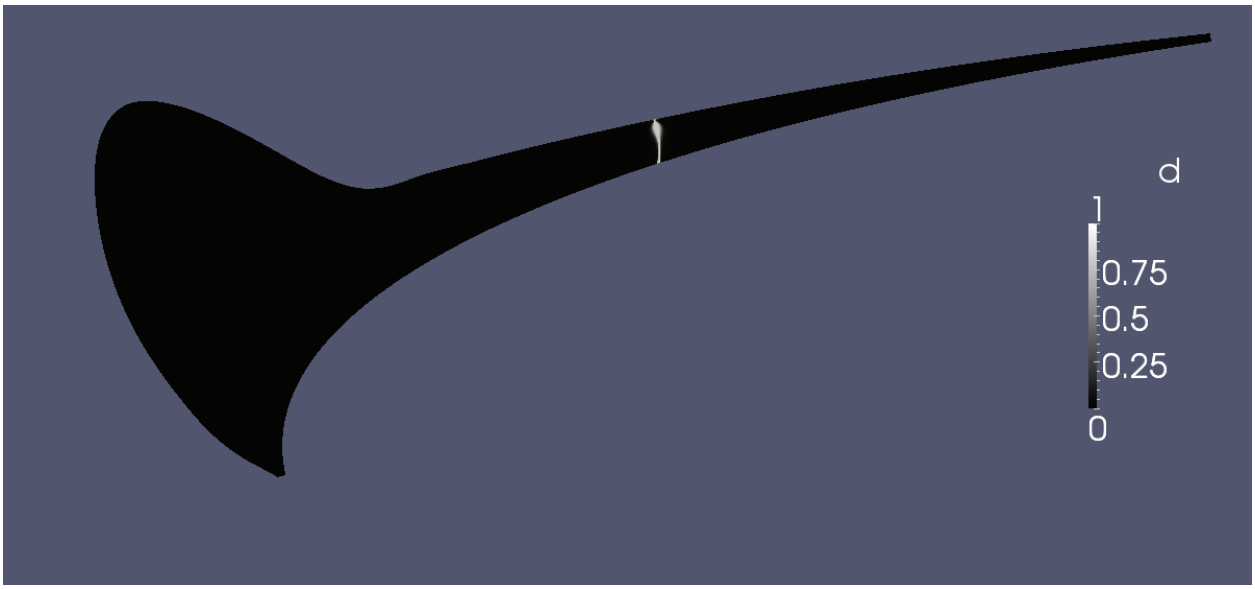

Figure 12. Global view of the fractured ice block

VII. Conclusion and perspectives

Firstly, we have presented the thermal models and the results they give (coupled or alone). A first step of validation shows that they correctly predict the thermal fields when used individually. A next step will be to perform different academic test cases to span all possible prototype problems. But more importantly we need to compare the coupled computation with experimental results in order to completely assess the validity of the approach.

Secondly, we have demonstrated the feasibility of ice shedding prediction using a new methodology of crack propagation. However this approach remains to be experimentally validated on simple cases as much as on complex de-icing cases.

The next step will now be to integrate these modules into IGLOO2D, the 2nd generation ONERA icing toolbox. Once that will be done, it will be possible to perform a realistic simulation of a complete de-icing cycle in flight conditions. The results of such a computation will be compared with experimental data.

Acknowledgements

The work presented in this communication was realised in the context of an Airbus/ANRT CIFRE grant. We gratefully acknowledge their support. We also wish to thank F. Dezitter, J. Cliquet and M. Logeais for the helpful discussions we had.

References

[1]V. Alexiades A.D. Solomon. *Mathematical modelling of melting and freezing processes*. Hemisphere, 1993.

[2]M. Farzaneh A.M.A. Mohamed. An experimental study on the tensile properties of atmospheric ice. *Cold regions science and technology*, 68, 2011.

[3]G.A. Francfort B. Bourdin and J.M. Marigo. The variational approach to fracture. *Journal of Elasticity*, 91, 2008.

[4]J.E. Bolander and S. Saito. Fracture analyses using spring networks with random geometry. *Engineering Fracture Mechanics*, 61(5-6), 1998.

[5]M. Hofacker C. Miehe and F. Welschinger. A phase field model for rate-independant crack propagation robust algorithmic implementation based on operator splits. *Computer Methods in Applied Mechanics and Engineering*, 2010.

[6]P. Duval E. M. Schulson. *Creep and fracture of ice*. Cambridge University Press, 2009.

[7]M. Eskandarian. *Ice shedding from overhead electrical lines by mechanical breaking*. PhD thesis, Universite du Quebec a Chicoutimi, 2005.

[8]J. Perron G. Fortin. Ice adhesion models to predict shear stress at shedding. *Journal of adhesion science and technology*, 26:523–553, 2012.

[9]R. Henry. Development of an electrothermal de-icing/anti-icing model. In *AIAA 30th meeting, Reno, NV (USA)*, 1992.

[10]V. F. Petrenko I. A. Ryzhkin. Physical mechanisms responsible for ice adhesion. *J. Phys. Chem. B*, 101, 1997.

[11]J. L. Laforte J. Druez, C. L. Phan and D. D. Nguyen. The adhesion of glaze and rime on aluminium electrical conductors. *Transactions of the CSME*, 5(4), 1978-79.

[12]A. Benallal J. Lemaitre, J.L. Chaboche and R. Desmorat. *Mecanique des materiaux solides*. Dunod, 2009.

[13]H. H. G. Jellinek. Ice adhesion. *Canadian journal of physics*, 1962.

[14]H. H. G. Jellinek. Liquid-like (transition) layer on ice. *Journal of colloid and interface science*, 1967.

[15]M. Farzaneh M. Kermani and R. Gagnon. Bending strength and effective modulus of atmospheric ice. *Cold regions science and technology*, 53, 2008.

[16]M.R.M. Aliha M.R. Ayatollahi and H. Saghafi. An improved semi-circular bend specimen for investigating mixed mode brittle fracture. *Engineering Fracture Mechanics*, 78(1), 2011.

[17]M. J. Clouter P. H. Gammon, H. Kiefte and W. W. Denner. Elastic constants of artificial and natural ice samples by brillouin spectroscopy. *Journal of glaciology*, 29((103)):433–460, 1983.

[18]M. Chu R. Scavuzzo and V. Ananthaswamy. Influence of aerodynamic forces in ice shedding. In *29th aerospace sciences meeting and exhibit*, 1991.

[19]R. A. Khurram S. Zhang, O. El Kerdi and W. G. Habashi. Fem analysis of in-flight ice break-up. *Finite elements in analysis and design*, 57, 2012.

[20]M. E. R. Shanahan. Adhesion and wetting: similarities and differences. *Rubber world*, 205, 1991.

[21]J. R. Shewchuk. Triangle: Engineering a 2d quality mesh generator and delaunay triangulator. In D. Manocha M. C. Lin, editor, *Applied Computational Geometry: Towards Geometric Engineering*, volume 1148 of *Lecture notes in computer science*. Springer-Verlag, 1996.

[22]J. H. VanSant. *Conduction heat transfer solutions*, 1980.

[23]T.G. Keith W. B. Wright and K.J. De Witt. Numerical simulation of icing, de-icing and shedding. In *29th Aerospace Sciences Meeting, Reno, Nevada, AIAA-91-0665*, 1991.